The Electronic Properties and Applications of Quantum Wells and Superlattices of III-V Narrow Gap Semiconductors

R. A. Stradling,
Blackett Laboratory,
Imperial College of Science, Technology & Medicine,
London SW7 2BZ, UK.

Received July 21, 1995

A tutorial review is given of the transport, the electronic and optical properties and the applications of quantum wells and superlattices which can be formed from III-V narrow gap struclures containing antimony.

I. Introduction & Electronic Properties

The most developed low-dimensional semiconductor structures, both for fundamental studies and in device applications, are those based on abrupt heterostructures between GaAs and AlGaAs. This system depends for its success on the near-perfect match between the binary components, GaAs and AlAs. However, GaAs does not have a band- gap suitable for long-wavelength optical sources, signal processing devices or mid- infrared detectors. There are also potential applications for narrow gap materials for fast signal processing and for a electrical sensing devices. These developments have produced dermands for new materials based on InAs, InSb and GaSb. The primary electronic characteristics of these systems are their high mobilities, and saturation drift velocitics, the band gaps which correspond to the infrared region of the spectrum and the low effective masses which give high quantum confinement energies. The latter characteristic opens up the possibility of the observation of mesoscopic and Coulomb blockade effects at higher temperatures. This paper reviews recent work carried out at Imperial College with MBE grown samples. The heterostructure combinations of particular interest are InAs/In($As_{1-x}Sb_x$), InSb/In($As_{1-x}Sb_x$), InAs/GaSb and InAs/AlSb.

InAs has a very low lying conduction band which leads to the formation of type II band alignments at heterojunctions and to very large conduction band offsets which can be exploited in such devices as tunnel diodes. The type II alignment can drastically modify the electronic properties; e.g. by leading to the suppression of Auger recombination. Another special property is that the deep lying conduction band causes native defect levels to lie about 200meV above the conduction band edge rather than in the middle of the forbidden gap[1-3]. Consequently electron accumulation layers form naturally at the surfaces of bulk layers and the Fermi energy at a metal semiconductor contact is pinned within the conduction band at a similar energy. Thus a Schottky barrier is not present and contacts which are extremely transparent to electron flow are readily formed.

The defect levels which cause the surface pinning also act to stabilise the Ferrni level which provides an electronic reference level for the defect annihilation energies. In the case of amphoteric impurities this determines the maximum free carrier concentration which can be obtained from doping[1]. Consequently InAs can be doped very heavily with Si donors where concentrations as high as $5 \times 10^{19}\text{cm}^{-3}$ can be achieved. With GaAs, where the Fermi level is pinned mid-gap, the donor doping limit is $\simeq 10^{19}\text{cm}^{-3}$. With InSb the pinning energy is near to the valence band so Si acts amphoterically but almost complete activation of the silicon as a donor up to concentrations of $3 \times 10^{18}\text{cm}^{-3}$ can be obtained by reducing the temperature in MBE

growth to 350°C. With GaSb and AlSb silicon only acts as an acceptor. These trends can be understood qualitatively in terms of the amphoteric native defect model introduced in Ref. [1] where the defects act to stabilise the Fermi level. The position of the defect levels with respect to the band edges therefore determines the maximum free carrier concentration which can be obtained by silicon doping. The defect levels lie in the conduction band of InAs but close to the valence band edge in GaSb.

I.1 $InAs_{1-x}Sb_x$

$InAs_{1-x}Sb_x$ alloy with $x \sim 0.65$ has the narrowest direct band gap of any thick-film III-V system. Remarkably, when InSb is mixed together with the wider band gap material InAs at low compositions, the band gap narrows. Unfortunately the alloy is prone to metallurgical problems such as ordering and phase separation in the mid alloy range and even natural superlattices can be grown when material is supplied at constant composition. High mobility strain-layer superlattices of both $InAs/InAs_{1-x}Sb_x$ and $InSb/InAs_{1-x}Sb_x$ have been grown despite the large mismatch.

I.2 InAs/GaSb and InAs/AlSb systems

InAs/GaSb/AlSb provides attractive combinations for both infrared and electronic applications. In the case of InAs/GaSb, the InAs conduction band minimum lies lower than the top of the GaSb valence band (type III alignment) so the system is naturally semimetallic leading to the possibility of novel electron-hole states. The InAs/AlSb system has an exceptionally high conduction band offset (1.6eV) particularly suited to tunnel and other microelectronic devices.

The untreated GaSb surface is known to produce donor like levels which act to pin the Fermi energy at the surface about 0.2 eV above the valence band edge[5,6]. The surface donors provide an additional source of electrons for the InAs quantum well above the intrinsic concentration arising from the semimetallic band alignment with the concentration of extra electrons varying approximately inversely with the thickness of the GaSb cap [5].

A particular problem arises with InAs/AlSb devices because of the instability in air of AlSb. In order to prevent corrosion, the final AlSb layer has to be capped by either a thin GaSb or InAs layer. When GaSb is employed the Fermi energy is pinned by the surface donors. Alternatively an $Ga_{1-x}Al_xSb$ alloy with $x \gtrsim 0.5$ can be used as an air-stable cap.

There is no common anion or cation across the interface between InAs and GaSb (or AlSb). It is therefore possible to induce two different types of bonding, InSb-like or AlAs (or GaAs)-like at the interface by careful control of the shutter sequences. Without such control the bonding at the interfaces will be random. The band offsets, the local vibrational properties and the electronic mobilities will depend on the nature of the interfaces

Generally samples grown with AlAs (GaAs)-like interfaces have inferior structural quality and much lower mobility than those with InSb interfaces[6]. The problem appears to be the roughening of the surface during the growth of the first AlAs (GaAs) interface due to the exposure of the AlSb (GaSb) surface to excess As. There have been reports that this problem can be overcome by the use of a cracker cell. By reducing the As pressure to the minimum level required to grow good quality InAs and by growing at low temperatures (~400°C) we can obtain 4K mobilities up to 200,000cm/Vs with GaAs-interfaces without the use of a cracker cell[7]. The optimum temperature for obtaining high mobility with InSb-interfaces is about 450°C.

I.3 The Remote doping of InAs/GaSb quantum wells by means of a second InAs well doped with silicon

Remote doping of InAs/GaSb or InAs/AlSb quantum wells presents a problem with molecular beam epitaxy (MBE). Use of a group VI dopant risks long term memory effects. Silicon, which is the preferred MBE dopant for most other III-V systems, acts as an acceptor with GaSb and in AlSb.

An alternative technology has been developed [8] for remote doping of the InAs quantum wells (see Fig. 1) where a double well structure is employed. The second InAs well is thin (~ 2nm) and doped with silicon where concentrations as high as $5 \times 10^{19}cm^{-3}$ can be employed (see section I). Because of the high confinement energy this well acts as a source of electrons for the

first well. As can be seen from table one mobilities as high as 185,000 cm^2/Vs with a carrier concentration of $2.68 \times 10^{12}\,cm^{-2}$ can be achieved in the wide well. The conductivity in this case is 10^{-1}S. Higher electron concentrations are possible but the mobility falls when the second subband becomes occupied, probably due to intersubband scattering. The parallel conductance from the thin well is negligible. A self-consistent modelling programme has been developed to describe the electron transfer. The model includes i) the nonparabolicity of the InAs conduction band, ii) the hole 2DEGs in the GaSb and iii) the surface pinning of the Fermi energy due to the presence of surface donors in the GaSb. The modelling predicts that we can achieve even higher carrier concentrations in the high mobility channel without degrading the mobility by using even thinner ($\sim$ 1nm) doping wells.

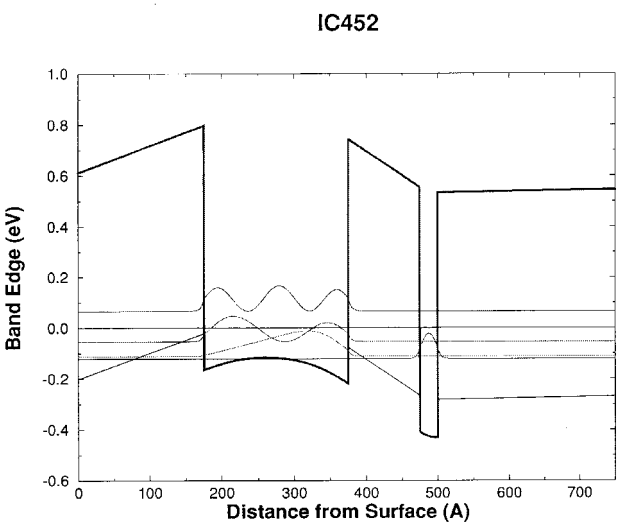

Figure 1. Illustrates the principle of the doping well technique where a thin highly- doped well is used as a source of electrons. The high confinement energy causes the electrons to transfer to the wider well.

I.4. Mesoscopic Properties

Two clear advantages of narrow gap materials over other semiconductor systems have been identified for mesoscopic studies. The increased energy separation of the 1- or 0-D subbands means that mesoscopic effects can be followed to substantially higher temperatures it should be possible to follow effects to about three times higher temperature for a particular feature size if InAs/(AlGa)Sb rather than GaAs/(AlGa)As is employed for a given structure. Thus Inoue et al[9] were able to observe the quantised conductance of an InAs/(AlGa)Sb split-gate quantum wire device up to 80K. The second advantage identified by Koester et al[10] is that ballistic effects can be observed to longer channel lengths; e.g. fully ballistic quantised conductance was observed with a channel length of 1μm. It was thought that this enhanced length performance arose because the subband separation was greater than the amplitude of the potential fluctuations in the wire.

We have prepared a series of InAs/GaSb quantum wires using e-beam lithography and wet etching down to 0.3μm width using a "doping well" sample as described in section I.3 with a carrier concentration of $2.7 \times 10^{12} cm^{-2}$ and 4K mobility of 185,000cm^2/Vs and observed the giant weak-field magnetoresistance reported in Ref. [11] which is enhanced by high carrier concentrations.

II. Optical properties

II.1 Raman Scattering from Plasmon Modes in Narrow Gap Semiconductors

Raman measurements of the plasmon frequencies provides a simple, accurate and non- invasive determination of the concentrations and mobilities of the charge carriers in semiconductors. The main features of the plasmon-LO phonon interaction are well established for 3-D systems. Two coupled modes are seen in Raman and FIR measurements with the L_+ mode occurring at the LO phonon frequency in the limit of low carrier concentrations and progressively changing character to become the plasmon mode at high carrier concentrations. The L_- mode approaches the TO phonon frequency in the limit of high carrier concentrations. A detailed Raman study[12] however shows unexpectedly that the L_- branch approaches the TO frequency asymptotically from the high frequency side as the carrier concentration increases. This behaviour is attributed to competition between screening (dominant at high frequencies) and a large-wavevector induced decoupling.

The widths of the plasmon modes observed by Raman and FIR spectroscopy can provide information about the mobility of the carriers. With our bulk

Table 1: A comparison between experimental and theoretical carrier concentrations obtainable with InAs/GaSb quantum wells by remote doping with a second well which is thin and highly doped.

Sample	Electron Density (x1e11cm^{-2}) *Theory* subband 1	2	Total	*Experiment* subband 1	2	Total	*Difference* %	Mobility (cm^2/V.s)
Single Wells								
IC411	12.3	2.5	14.8	13.6	3.7	17.3	14	90,000
IC404	9.3	0.7	10.0	9.5	-	9.5	5	200,000
IC410	7.4	-	7.4	8.2	-	8.2	10	100,000
Double Wells								
IC452	16.1	7.4	23.5	15.9	5.9	21.8	8	155,000
IC455	24.4	5.7	30.1	22.8	(4.0)	(26.8)	12	185,000
IC463	19.2	9.6	28.8	21.2	8.9	30.1	4	50,000
IC475	25.3	8.1	33.4	28.4	7.2	35.6	6	70,000
IC497	23.4	4.8	28.2	20.8	-	20.8	36	180,000

$InAs_{1-x}Sb_x$ alloys the mobility in samples without deliberate doping degrades rapidly as the composition (x) is changed from either end of the system (x=0 and x=1) and also falls off rapidly with decreasing temperature. This mobility degradation cannot be explained by chemical contamination, particularly as samples heavily doped with silicon have higher temperature independent mobilities. Insight into the reason for this behaviour is provided by the scattering times deduced from the widths of the plasmon modes observed which are several times narrower than expected from the dc mobility. The explanation for the degradation of the dc mobility in the undoped samples appears to be that a mobility edge occurs, possibly because of the metallurgical effects referred to in section I.1. The optical transitions are "vertical" and are therefore unaffected by the fluctuations in potential on a scale larger than the de Broglie wavelength which give rise to the mobility edge.

Several new peaks are observed in resonant Raman scattering from GaSb/InAs[13] and AlSb/InAs quantum wells[14,15]. These lines are assigned to the coupled LO phonon-intersubband plasmon modes originating from the InAs wells[13]. The lower frequency branch of the coupled system (L_- mode) lies between the LO and TO frequencies of InAs, and the line intensity depends strongly on the two dimensional carrier concentration and the laser excitation energies (chosen to be near to resonance with the E_1 gap of InAs). The L_+ lines are weak and relatively broad, their frequency increases with increasing carrier concentration in the InAs wells and they are not observed when the carrier concentration is low (figure two and three). If the InAs conduction band is parabolic then the energies of the main L_- and L_+ modes can be derived from

$$E_\pm = \frac{1}{2}(E_{12}^2 + E_{LO}^2 + E_P^2) \pm \frac{1}{2}[(E_{12}^2 + E_{LO}^2 + E_P^2) - 4(E_{12}^2 E_{LO}^2 + E_{TO}^2 E_P^2)]^{1/2}$$

where E_{12} is the energy spacing between the first and second electron subbands and E_P is the polarisation shift associated with the intersubband plasmon energy.

The main application of intersubband scattering lies in that the technique allows a relatively simple determination of the energy separation between subbands. The main scientific interest for narrow gap semiconductors is in the nonparabolicity corrections. We have studied the L_- and L_+ coupled plasmon-phonon intersubband modes also with $InAs/InAs_{1-x}Sb_x$ strained layer superlattices.

Figure two shows also an L_+ mode associated with

transitions from the second subband. Figure three demonstrates a shift to higher frequency with increasing carrier concentration. These measurements were made with the carrier concentrations increased by the "doping well" technique.

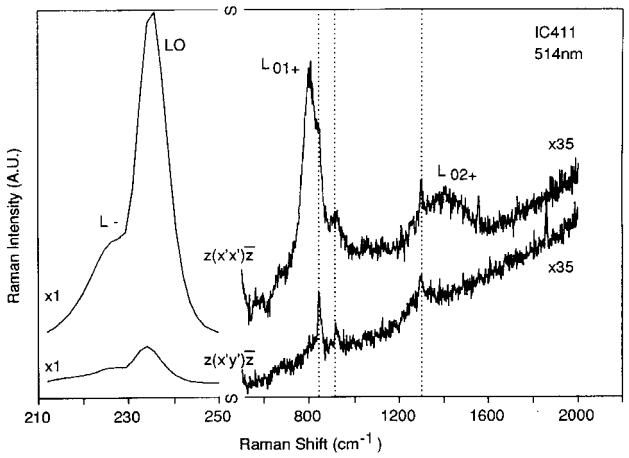

Figure 2. Shows the Raman spectrum from an InAs/GaSb single quantum well. The L_- mode is observed just below the main LO phonon peak (a composite of the InAs and GaSb phonons). Above 750cm^{-1} the gain is increased by 35 and two L_+ peaks are seen corresponding to the transitions from the lowest subband to the first two of the higher subbands.

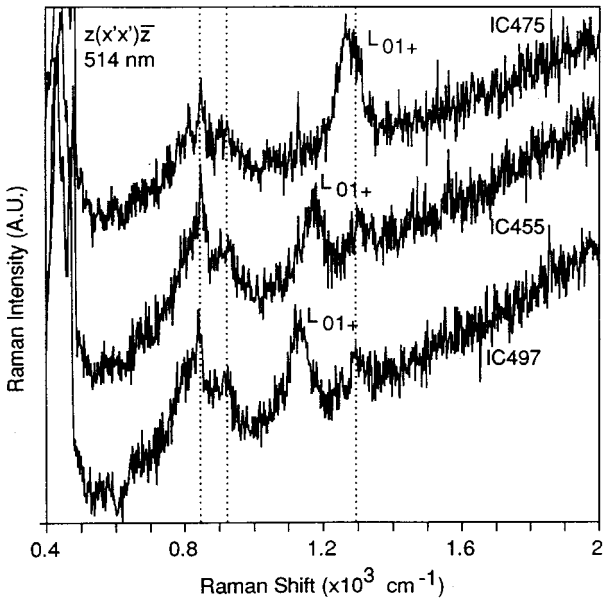

Figure 3. Shows the Raman spectrum from three InAs/GaSb single quantum well with different carrier concentrations. The L_+ mode corresponding to transitions from the lowest subband to the first of the higher subbands increases in energy with increasing carrier concentration.

II.2 Structural characterisation of semiconductor structures by Raman spectroscopy

We are exploring Raman techniques for non-destructive and rapid characterisation of a variety of electronic materials and device structures. Applications for characterisation include the simple determination of alloy composition, local strain, the folded phonon modes in the case of superlattices which provide information on the quality of the superlattice structure, and interface integrity which can involve, in the case of the InAs/GaSb and InAs/AlSb, the detection and analysis of the InSb and GaAs-like interface modes.

II.3 Interband magneto-optics in InAs/InAs$_{1-x}$Sb$_x$ superlattices

Interband magneto-optical measurements show many more transitions than luminescence studies because excited states in both the conduction and valence band wells are involved. Consequently magneto-optics can be extremely powerful in determining the complete set of band structure constants[16] and band offsets[17].

We have investigated by interband magneto-optics the band alignments of a series of InAs/InAs$_{1-x}$Sb$_x$ strained layer superlattices of the same composition $0 \leq x \leq 0.4$ used for studies of photoluminescence and electroluminescence[17]. Luminescence, by ourselves and also by other groups, shows that the photon energy emitted falls extremely rapidly with increasing x with the band gap decreasing from 0.4 eV for x = 0 to 0.1 eV for x=0.4 (Fig. 4).

The reason for this rapid narrowing of the superlattice energy gap has been controversial with different groups suggesting conflicting schemes; (i) extreme "type II" band alignments with the valence band offsets changing rapidly with x (in which case the photon emission is spatially indirect) or alternatively (ii) a spatially direct band gap in which the alloy band gap is anomalously narrowed by microstructural effects such as atomic ordering. Our data provide an unambiguous assignment for the band offsets as the peaks can only be fitted with the type II band alignments. However it is still unclear whether a model involving placing the

InAs band lower than the alloy or the reverse ordering (Fig. 5) is more appropriate

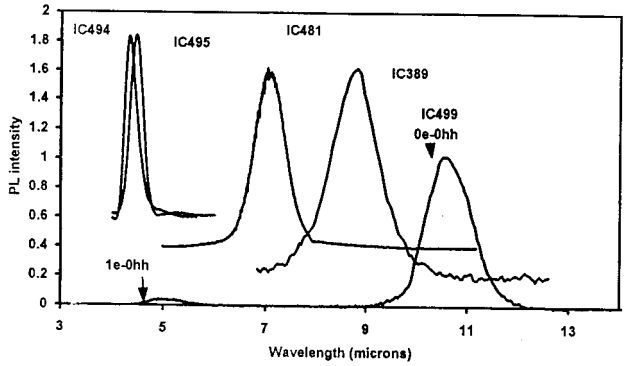

Figure 4. Shows the narrow high-efficiency photoluminescence at 12K from four InAs/$InAs_{1-x}Sb_x$ strained layer superlattices with x = 0, 0.2, 0.32 and 0 4. Thus increasing the average antimony content of the structures by only ~20% shifts the luminescence peak by a factor of three in wavelength.

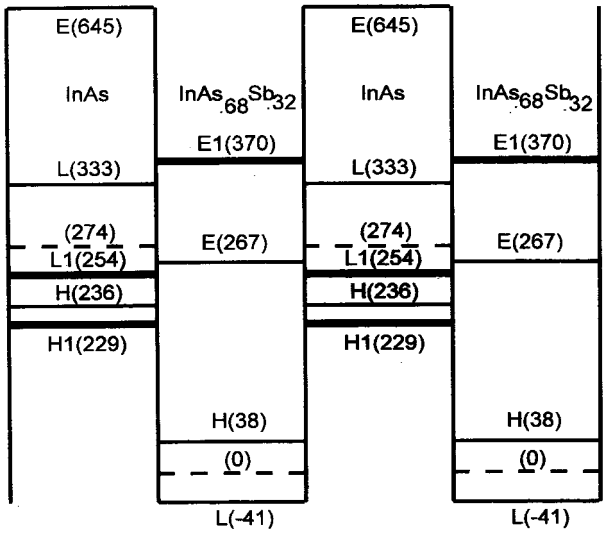

Figure 5. Shows the schematic band alignment which provides the best fit for the interband magneto-optics for InAs/$InAs_{1-x}Sb_x$ strained layer superlattices with x= 0.32. E1, L1 and H1 are the first quantum confinement states; E, L and H are the band extremes and the dashed lines correspond to unstrained values. All energies are in meV.

II.4 Magneto-optical and transport measurements with gated InAs/GaSb quantum well structures

Gated Hall effect and capacitor structures showing a good field effect have been fabricated on wafers containing InAs/GaSb quantum wells using MOS techniques with the SiO_2 being deposited either by a low temperature photolytic process (in collaboration with DRA Malvern) or a plasma assisted chemical vapour process (in collaboration with the University of Hamburg). The structures consisted of a single InAs quantum well located about 20nm from the SiO_2/GaSb interface. Reproducible breakdown characteristics were obtained with both processes with breakdown fields in the oxide of up to 5×10^6 V/cm. The field effect in the InAs/GaSb structures is extremely good for intermediate gate voltages with the electron concentration changing between 0.8 and 2.2×10^{12} cm^{-2} as measured by the Hall effect. The low temperature mobility increases from 40,000 cm^2/Vs at negative bias to 135,000 cm^2/Vs for a bias of +40V. These results suggest that mobilities near to the phonon limited value of 30,000 cm^2/Vs should be achievable at room temperature in FET structures using SiO_2 gates.

We have therefore demonstrated a viable technology for InAs/GaSb/AlSb MOS field effect devices.

The field effect in the capacitor structures was also monitored by cyclotron resonance. The amplitude and half width of the CR transmission minima generally show a strong oscillatory behaviour with magnetic field (Fig. 6). This can be interpreted in terms of the variation of the screening on the electron occupancy of the Landau levels[18] or because of the movement of the Fermi energy through the Landau levels which can change the weightings of individual inter-Landau level transitions which differ in energy because of nonparabolicity[19–23]. The ability to change the carrier concetration controllably by means of the gate shows that both these mechanisms play a role in determining the line shape. At negative and low positive gate biases the CR line is broadens when the Fermi energy lies between two Landau levels. As the gate voltage (carrier concentration) increases, the oscillations in the line width decrease and disappear at one particular gate voltage. At higher gate voltages the oscillations reappear but with opposite phase; i.e. when the line width is greatest when the Fermi energy lies within a Landau level at the position of a maximum in the density-of-states function. When the line width is near to its minimum value the individual inter-Landau level transitions become resolved (Fig. 7). This observation therefore suggests that the second mechanism is operative at high electron concentrations.

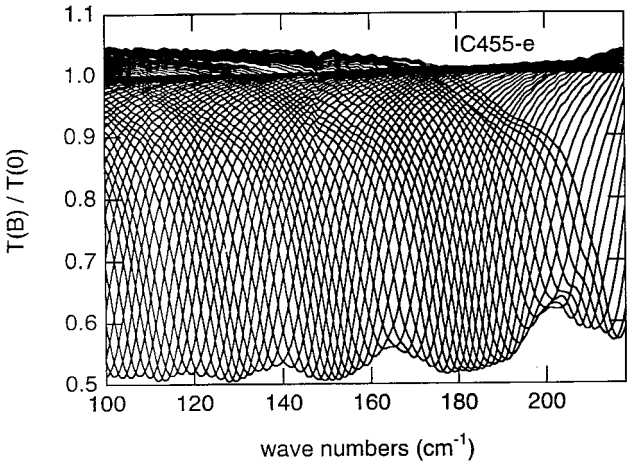

Figure 6. Shows cyclotron resonance absorption lines taken at intervals in magnetic field of 0.2T for an InAs/GaSb single quantum well. The intensity and inverse line width shows Shubnikov-de Hass like oscillations which are periodic in 1/B.

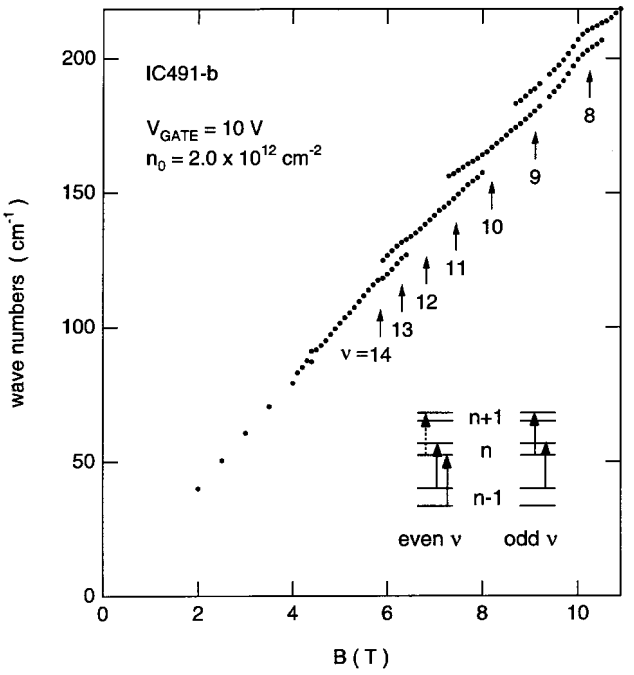

Figure 7. Shows the magnetic field positions of the cyclotron resonance absorption lines for a gated InAs/GaSb single quantum well. Above about 6T the individual transitions making up the cyclotron absorption become resolved.

Because of the very high Fermi energies, the effective mass measured with large positive gate biases increases by more than a factor of two compared with the band edge mass of InAs. This demonstrates the extreme importance of non-parbolic corrections in these narrow gap systems.

The semimetallic band alignments with InAs/GaSb heterostructures lead to the simultaneous presence of electrons and holes in undoped strucures. There has been considerable speculation for some time that such a system could lead to the formation of stable excitonic states at low temperatures. Experimental evidence for such states has been lacking until recently when Cheng et al[24] reported the presence of an additional line approximately 2 meV above the cyclotron resonance line in a number of InAs/(Ga,Al)Sb quantum wells which disappeared with increasing temperature. In this experiment the persistant photoconductive effect was used to control the carrier concentration and the line was only present when the electron and hole concentrations were approximately equal. In our own experiments with gated InAs/GaSb structures we were unable to obtain convincing evidence for the existence of such an excitonic related line although we were able to observe a line with approximately the same magnitude of energy offset from the cyclotron resonance line *but of differing sign* (i.e. on the low energy side of the main CR) with a strongly n^+ "doping well" sample. Warburton et al[23] also observed a similar line with a heavily p^+ sample and they interpreted this as a splitting arising from spin-orbit coupling arising from the lack of inversion symmetry.

The Shubnikov de Haas oscillations in the resistance could be observed at magnetic fields as low as ~0.5T near zero bias and ~1.5T even at large positive gate voltages where the fundamental fields were ~50T. The observation of such high Landau indices ($n \sim 30$) corresponding to filling factors (v) of ~60 implies that the gate induced 2DEG is extremely laterally homogeneous. The peaks were analysed using fast Fourier transform techniques to derive the electron concentrations. Above a gate bias of ~10V the Shubnikov de Haas measurements show clearly that the second electron subband is occupied with concentrations between 3 and 6×10^{11} cm^{-2}. Extrapolation of the observed bias dependence suggests that this subband first becomes occupied at about 0V applied to the gate. The sum of the first and second subband concentrations agrees rather accurately with the value of carrier concentration derived from the four parameter fit to the classical Hall and magnetoresistance measurements.

The appearance of an extra peak in the Fourier spectrum is linked with the observation of a beating pattern

superimposed at relatively low fields on the Shubnikov-de Haas peaks (see Fig. 8). Similar beating patterns have been reported previously for InAs/GaSb quantum wells[25] and for GaAs/AlGaAs structures[26–28]. In Ref. [25] the beating was attributed to the lifting of inversion symrnetry in the well by electric field induced terms whereas in the case of the GaAs/AlGaAs samples the new structure was believed to result from the occupancy of the second subband.

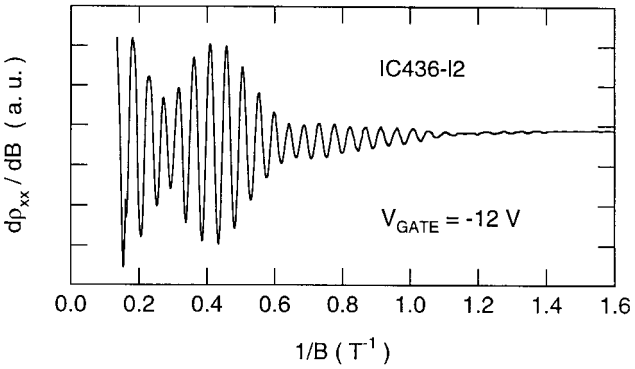

Figure 8. Shows the beating pattern superimposed on the Shubnikov de Haas oscillations (dR/dB) for a gated InAs/GaSb single quantum well.

The fact that the additional peak in the Fourier spectrum appears so strongly in our gated samples favours the electric field induced mechanism. Peak B_X appears to split off from the main strongest Fourier peak and in this sense could be mistaken for the peak arising from the difference between the occupancies of the first and second subbands. However the position is quite different and mixing peaks from both the second subband and peak B_X can frequently be observed (as can be seen from Fig. 9). The peak can frequently be seen in Fourier spectra of ungated samples but is generally of weaker amplitude. The peak is not thought to be be hole related as the concentration required would be some four times greater than that expected at a single interface. Electron accumulation at the GaSb/SiOx interface can be ruled out as the peak appears close to zero bias applied to the gate. A more likely explanation is in terms of an electric field induced spin-splitting brought about by spin-orbit coupling as discussed in Refs. [25, 29 and 30]. This term should be stronger in the gated structures the internal electric fields are generally weaker in the ungated samples, e.g. the fields at the opposite interfaces are of different sign with the remotely doped structures investigated[8]. The advantage of the gated structures for a study of such electric field induced effects is obvious in that the induced peak can be studied systematically as a function of electric field for a single structure.

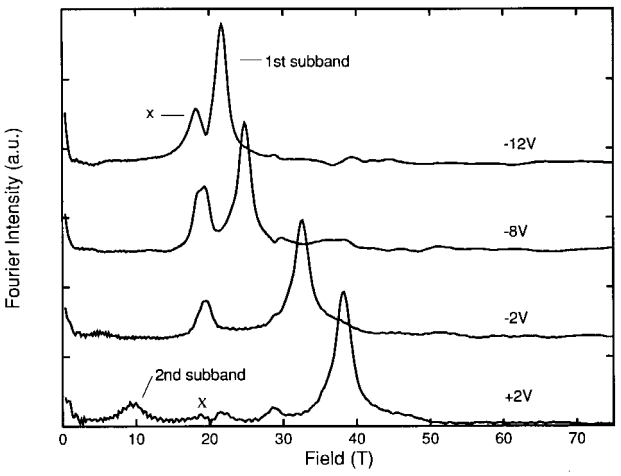

Figure 9. Shows the Fourier transform of beating patterns observed in the Shubnikov-de Haas peaks for a gated InAs/GaSb single quantum well as a function of increasing gate bias. The separation in magnetic field of the main doublet increases with applied electric field (carrier concentration). This behaviour is consistent with an electric field induced spin-orbit effect.

II.5 Non linear optics with the free electron laser - FELIX

Free electron lasers (FEL's) offer an unrivalled combination of wide, rapid and continuous tunability, high peak power ($\sim$ 1 MW cm^{-2}) and controllable high (ps) time resolution. In the far infrared (FIR) region other systems give only sparse coverage and do not have the time resolution. The Dutch FEL at Utrecht (FELIX), is a unique "user facility", giving laser output for time resolved spectroscopy spanning the 5 to 110 μm wavelength range. There is a major collaborative programme from the UK, of which we are part, in nonlinear and time-resolved studies in the mid-infrared of semiconductors using FELIX.

The first measurements conducted in the collaborative programme which involved ourselves and Heriot-Watt University were on MBE films of InSb grown on GaAs. Using the FEL it was possible to obtain results over a much wider range of excited carrier densities, n, than obtained previously by less direct methods. The different scattering regimes were clearly observed, from Shockley-Read (carrier concentration independent) lifetimes at low excitation intensity, through an n-squared

dependence at intermediate concentrations consistent with non-degenerate Auger scattering, to a linear n dependence at high concentrations, as expected for degenerate Auger scattering.

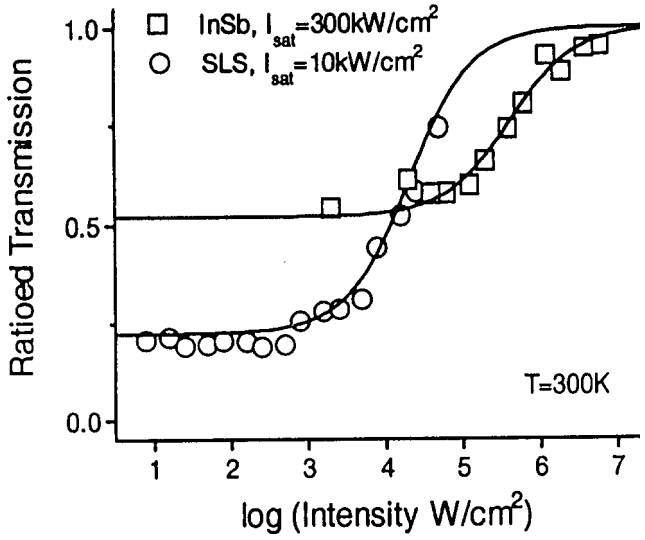

Figure 10. Shows dramatic results taken with a Free Electron Laser for the bleaching of interband absorption in As-rich InAs/$InAs_{1-x}Sb_x$ strained layer superlattice (SLS). In comparison the power needed to saturate bulk InSb is about thirty times greater.

This work has been extended to the much more interesting long wavelength heterostructures grown by MBE at Imperial College (the InAs/$InAs_{1-x}Sb_x$ system). In particular, Fig. 10 shows dramatic results for the bleaching of interband absorption in As-rich alloys of InAs/Sb strained layer superlattices (SLS). This is consistent with extremely strong room temperature photoluminescence observed experimentally for the first time between 4 and 11 microns, and is a direct demonstration of the results of 'band structure engineering', where the Auger processes have been deliberately suppressed by creating a type II strained layer superlattice structure. In comparison with the Auger lifetime obtained from similar measurements on InSb (room temperature bandgap about 7μm), the lifetime deduced from an alloy, whose measured bandgap was 11 μm, was some 50 times longer. Fig. 11 shows the results of pump-probe measurements which measure directly the room temperature lifetime of an InAs/$InAs_{1-x}Sb_x$ SLS and also of state-of-the-art cadmium mercury telluride detector following excitation at two different above-band-gap energies. Again the SLS outperforms the bulk material. These measurements represent the longest room temperature lifetime yet measured for a III-V semiconductor, either in bulk or heterostructure form.

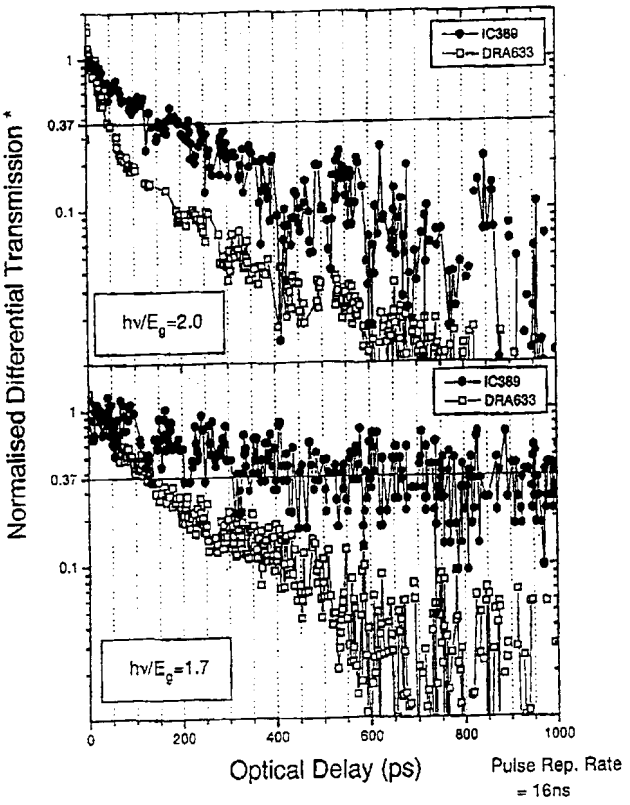

Figure 11. Compares the results of pump-probe measurements taken with the Free Electron laser (FELIX) which measure directly the room temperature lifetime of an InAs/$InAs_{1-x}Sb_x$ SLS and also a cadmium mercury telluride detector following excitation with above-band-gap energies. The lifetime for the InAs/$InAs_{1-x}Sb_x$ SLS is much longer.

We have also undertaken pump-probe studies of the cyclotron resonance and donor lines in bulk InAs. Fig. 12 demonstrates that the shallow donors take much longer to recover from near-saturation conditions than the free carriers and the capture time for the free carriers at the donors is $\sim$10ns.

III. Applications

A major area of development concerns infrared LEDs and lasers where there is an urgent requirement to provide low cost and sensitive systems for pollution monitoring where trace gases are to be detected by their fundamental vibrational-rotational absorption bands. There has been great progress recently in the development of III-V antimonide based lasers operating between 2 and 4 micron wavelength. The first report of operation with III-V antimonide materials sys-

tem was with bulk InSb where lasing was observed at a wavelength of 5.2μm but only below a temperature of 10K. Room temperature operation of lasers has been achieved at wavelengths as long as 2.8 microns and to 4.5 micron when cooled to liquid nitrogen temperatures. Table 2 lists the characteristics of mid IR laser systems which have been developed recently with III-V materials[33–46] and compares the results with II-VI ($Hg_{1-x}Cd_xTe$)[47,48] and IV-VI (PbSe/PbSrSe) laser systems[49]. Column one gives the institute and first author concerned and column two the materials system involved. Columns three to seven list the operating parameters at a particular temperature, column eight the structure and column nine the mode of excitation and the maximum operating temperature.

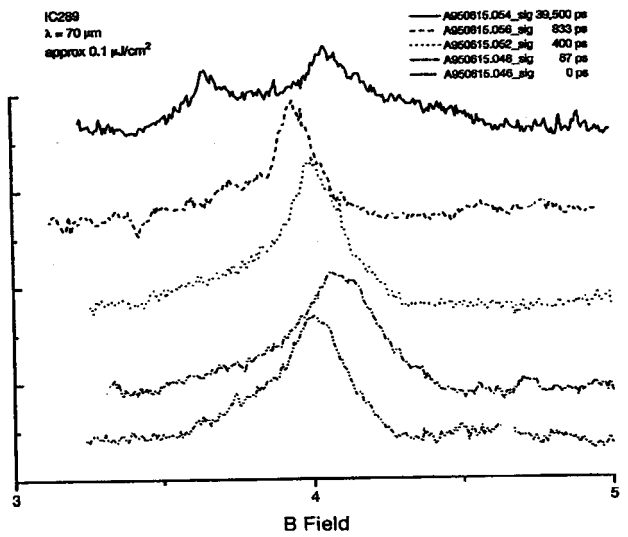

Figure 12. Shows the results of pump-probe measurements taken with a Free Electron laser which show the shallow donors (lower field peak) and the free carrier cyclotron resonance in bulk InAs. At short time intervals only the cyclotron resonance line is seen and this is much broadened. After times longer than lns the donor peak appears. The donors take much longer to recover from near-saturation conditions than the free carrier cyclotron resonance and the capture time for the free carriers at the donors is ~10ns.

In(As,Sb) has been used as a component in the active region of the laser structure at wavelengths between 3.4 and 4.5 microns in Refs. [35-38, 40]. We are studying infrared emission from MBE epilayers of InAs/In(As,Sb) grown in-house[42,43]. Our photoluminescence studies showed intense luminescence from these "strained layer superlattices" (where we use engineered band structure effects to quench non-radiative Auger recombination) and encouraged us to attempt to make practical light emitting diodes. We have observed significant emission at a wavelength as long as 9.8μm from an uncooled LED and have now made a number of LED devices emitting in the 4-10 μm spectral range.

The longest wavelength operation yet reported for a III-V laser at room temperature is at 2.78 μm where pulsed operation was achieved with a multiquantum well system with $In_{0.24}Ga_{0.76}As_{0.16}Sb_{0.84}$ wells and $Al_{0.25}Ga_{0.75}As_{0.02}Sb_{0.98}$ barriers[41]. The main problem preventing cw operation seems to have been an unexpectedly large series resistance, possibly from poor conductivity in the cladding layers.

In contrast pulsed operation very near to room temperature (282K) was very recently reported at 4.2 μm wavelength with lead salt multiple quantum well lasers ($PbSe/Pb_{0.9785}Sr_{0.0215}Se$)[49]. These authors suggest that IV-VI laser systems may be preferable to III-Vs for long wavelengths but that III-Vs are likely to be superior for wavelengths below 3 μm. The highest-temperature long-wavelength laser results with III-V materials are reported in Refs. [35] and [36] where 3.9 μm operation is achieved in the pulsed mode at 170K or at 210 K using optical pumping.

HgCdTe/ZnCdTe lasers have been made to operate pulsed at a wavelength of 5.3 μm up to 60K[47] and up to 154K at 3.2 μm wavelength using diode pumping[48].

A different approach, not involving band-to-band radiation is to use transitions between the subbands in a multiple quantum well structure[44,45]. A sophisticated (In,Ga)As/(Al,In)As superlattice structure is employed to obtain laser action where the lower state of the laser transition is separated by an optical phonon energy from the ground state to ensure population inversion. The electrons are recycled through twenty five stages and digital grading is designed to act as a Bragg reflector for the electrons in the excited laser state. The system is described as a "quantum cascade" laser. A simpler version of this structure is used for LED devices at longer wavelength. Operation at room temperature has yet to be achieved but laser emission at a wavelength as long as 8.4 μm was recently reported at temperatures up to 130K[46].

Narrow gap systems also give advantages for the low power/high speed operation of devices such as

Table 2: Performance of Near Infrared Laser/LED Systems

Group	Material	λ (micron)	Power	T	Threshold	To	Structure	Mode of operation
MIT	(GaInAl)(AsSb)	2	1.3W(cw)	300K	140A/cm2	110K	Broad stripe	
Choi [33-34]		2	100mW	300K	20mA		Ridge waveguide	
		2	200mW	300K			tapered	
		3	90mW	100K	9A/cm2 at 40K		DH	255K pulsed/cw to 170K
Le [35]	InAsSb/GaSb	3.9	0.8W	85K	optic pulse			210K optically pumped
Eglash [36]	InAsSb/AlInAs	3.9	30mW	70K			DH	170K pulsed/105K cw
	InAsSb/AlInAs	4.5						85K pulsed
	InAsSb/AlAsSb	4	200mW(mean)				DH/Diode Pumped	155K pulsed/80K cw
Sandia	InAsSb/InGaAs	3.9		< 100K			SLS	optically pumped
Biefeld/Kurtz [37]								
Ioffe	InAsSbP/InAsSb	3.2	8mW	80K	40mA	30K	DH	80K cw
Baranov [38]				180K	6A		(LPEgrown)	180K pulsed
Hughes	GaInSb/InAs	3.3		<170K			Type II SL	170K pulsed
Miles [39]		3.2						5K optically pumped
Hughes	InAs/AlAsSb	3					DH	
Zhang [40]	InAsSb/InAs	3.4		95K		32K	Diode pumped SLS	cw
Sarnoff Research Center *Lee [41]*	AlGaAsSb/ InGaAsSb	2.78	30mW	288K	10kA/cm2	58K	MQW	333K pulsed
ICSTM	InAs/InAsSb	3-10		290K			SLS LED	cw
Phillips [42,43]		4.5	~1μW					
		7	~0.2μW					
ATT	AlInAs/GaInAs			10K	1.7kA/cm2		cascade laser	
Capasso [44-46]								
		4.5	80mW	80K				pulsed
				100K	3kA/cm2			
		8.4	40mW	10K	2.1kA/cm2			pulsed
	AlInAs/GaInAs	8 to 13	6nW	10-200K			cascade LED (blue Stark shift)	cw
MIT	CMT/CdZnTe	3.2	1.3W peak	88K			QW	154K diode pumped
Le [48]			105mW mean					
Fraunhofer	PbSe/PbSrSe	4.2		282K	330mA		MQW	pulsed
Shi [49]		5	300μW	120K	800mA			cw
		7.3		30K				cw

DH = double heterostructure, SLS = strained layer superlattice, SL = superlattice, MQW = multiple quantum well

Field Effect Transistors (FETs) and Resonant Tunneling Diodes (RTDs). The high conduction band offset between InAs and AlSb (1.6 eV) make this combination particularly attractive for RTDs and the highest frequency operation yet achieved with any microelectronic device has been with an RTD InAs/AlSb device operating at 712 GHz[50,51]. Better high frequency response compared with InGaAs/AlInAs RTDs has been demonstrated though free electron laser studies at near terahertz frequencies[52]. Switching times as short as 1.7ps have also been measured directly by electro-optic sampling[53].

With FETs the attractive features of the InAs/AlSb combination are the very high saturation drift velocity for InAs and the high mobility together with the high room temperature resistance of AlSb which can be used for internal gates. A particular problem intrinsic with the use of a narrow gap material is impact ionisation. However Li et al[54] have shown that devices can be made to operate at channel electric fields (20kV/cm) well above the predicted threshold for impact ionisation. Three contributing processes were identified as possibly contributing to the suppression of impact ionisation. Firstly a complex barrier structure had been grown with these devices where holes generated in the breakdown process escaped from the InAs and were collected remotely at an AlSb/(Al,Ga)Sb interface. The loss of holes from the InAs well causes a reduction in the breakdown current. Secondly the gate length was less than the electron mean free path reducing the probability of an impact ionising collision significantly. Finally quantum confinement acts to increase the minimum energy gap in the InAs channel substantially. Bolognisi et al[55] showed that accumulation of holes in the barriers could lead to an undesirable "kink" effect in the device characteristics which could be avoided by the careful choice of composition for the (Al,Ga)Sb buffer. Microwave devices with a gate length of 0.5 μm have shown a peak unity current cut- off frequency (f_t) of 93 GHz. Structures with gates lengths as small as 0.2 μm

have been fabricated[56]. AlSb used as a gate insulator can withstand electric fields of 106V/cm (5V across 50 nm of AlSb) before breakdown occurs even with devices with such small gates[56].

Magnetic field sensors using Hall or magnetoresistance devices are currently being developed for automotive applications where temperatures up to 250°C may be experienced. A high field sensitivity is expected because of the high mobilities expected with narrow gap materials. However the intrinsic excitation of carriers across the band gap can provide a problem as this conflicts with the other design criterion for a magnetic field sensor for such applications which must have characteristics which change little with temperature. The use of delta doping or heterostructures involving InAs can keep the reduce the change in carrier concentration with temperature to acceptable limits and provide excellent performance[57].

Looking further forward to the future hybrid superconductor-semiconductor devices are becoming of increasing interest.

Acknowledgements

S. J. Chung, T. Knight, C. Langerak, Y. B. Li, T. Malik, J. Nehls, B. M. Murdin, A. G. Norman, C. C. Phillips, C. R. Pidgeon, M. Pullin, F. Rahman, P. Tang, T. Thornton, W. T. Yuen and R. Zallen have all contributed to the experiments reviewed in this paper. These contributions are gratefully acknowledged. EPSRC have provided the financial support for the growth of the structures used in these experiments and for much of the experimental work with these samples.

References

1. W. Walukiewicz Mat. Res. Soc. Symp. Proc. Vol **104**, 483 (1988) also Phys Rev. **37**, 4760 (1988).
2. C. Nguyen, B. Brar, H. Kroemer and J. H. English, J. Vac. Sci. Techn. B **10**, 898 (1992)
3. R. G. Egdell, S. D. Evans, Y. B. Li, R. A. Stradling and S. D. Parker Surface Science **262**, 444 (1992).
4. I. T. Ferguson, A. G. Norman, T. Y. Seong, R. H. Thomas, C. C. Phillips, X. M. Zhang, R. A. Stradling, B. A. Joyce and R. Booker, App. Phys. Lett. **59**, 3324 (1991).
5. G. Tuttle, H. Kroemer and J. H. English, J. App. Phys. **65**, 5239 (1989).
6. C. Nguyen, B. Brar, H. Kroemer and J. H. English, App. Phys. Lett. **60**, 1854 (1992).
7. S. J. Chung, A. G. Norman, W. T. Yuen, T. Malik and R. A. Stradling to be published in Proc. of 22nd Int. Symposium on Compoumd Semiconductors.
8. T. Malik, S. Chung, J. J. Harris, A. G. Norman, R. A. Stradling, and W. T. Yuen Int Conf. on Narrow Gap Semiconductors (Santa Fe) IoP Conference Series, **144**, 229 (1995).
9. M. Inoue, K. Yoh and A. Nishida, Semicond. Sci. and Techn. **9**, 966 (1994); also K. Yoh, H. Taniguchi, K. Kiyomi, M. Inoue and R. Sakamoto, EEE Technical Digest (IEDM 91 31.5.1) 1991.
10. S. J. Koester, C. R. Bolognisi, E. L. Hu, H. Kroemer and M J Rooks Phys Rev B **49**, 8514 (1994)
11. T. J. Thomton, M. L. Roukes, A. Scherer and B. P. Van der Gaag, Phys. Rev. Lett. **63**, 2128 (1989).
12. Y. B. Li, I. T. Ferguson, R. A. Stradling and R. Zallen, Semicond. Sci. and Techn. **7**, 1149-54 (1992).
13. Y. B. Li, V. Tsoukala, R. A. Stradling, R. L. Williams, S. J. Chung, I. Kamiya and A. G. Norman, Semicond. Sci. and Techn. **8**, 2205-2209 (1993).
14. G. Brozak, B. V. Shanabrok, D. Gamrnon, D. A. Broidp, R. Beresford and W. I. Wang, Phys. Rev. B **45**, 11399 (1992).
15. J. Wagner, J. Schmitz, F. Fuchs, J. D. Ralston, P. Koidl and D. Richards, Phys. Rev. B**51**, 9786 (1995).
16. S. N. Smith, C. C. Phillips, R. H. Thomas, R. A. Stradling, B. N. Murdin and C. R. Pidgeon, Semicond. Sci. and Techn. **7**, 900-906 (1992).
17. Y. B. Li, R. A. Stradling, A. G. Norman, P. J. P. Tang, S. J. Chung, and C. C. Phillips, Proc. 22nd Int Conf on Physics of Semiconductors (Vancouver) 1496-9 (1995).
18. D. Heitman, M. Ziesmann and L. L. Chang, Phys. Rev. B**34**, 7463 (1986).
19. E. B. Hansen and O. P. Hansen, Solid State Comm. **66**, 1181 (1988).
20. C. Gauer, J. Scriba, A. Wixforth, J. P. Kotthaus,

C. R. Bolognesi, C. Nguyen, C. Tuttle, J. H. English and H. Kroemer, Semicond. Sci. and Techn. **8**, S137 (1993).

21. M. J. Yang, R. J. Wagner, B. V. Shanabrook, J. R. Waterman, and W. J. Moore, Phys. Rev. B**47**, 6807 (1993).
22. C. Gauer, J. Scriba, A. Wixforth, J. P. Kotthaus, C. R. Bolognesi, C. Nguyen, B. Rrar and H. Kroemer, Semicond. Sci. and Techn. **9**, 1580 (1994).
23. R. J. Warburton, B. Brar, C. Gauer, A. Wixforth, J. P. Kotthaus and H. Kroemer. To appear in the Proceedings of MSS-7.
24. J. P. Cheng, J. Kono, B. D. McCombe, I. Lo and W. C. Mitchel, Proc. Int Conf on Physics of Semiconductors (Vancouver) p751 (Pub. World Scientific, 1995) also Phys Rev. Lett. **74**, 450 (1995).
25. J. Luo, H. Munekata, F. F. Fang and P. J. Stiles, Phys. Rev. B**41**, 7685 (1990).
26. T. P. Smith, F. F. Fang, U. Meirav and M. Heiblum, Phys. Rev. **38**, 12744 (1988).
27. D. R. Leadley, R. J. Nicholas, J. J. Harris and C. T. Foxon, Semicond. Sci. and Techn. **4**, 885 (1989).
28. P. T. Coleridge, Semicond. Sci. and Techn. **5**, 961 (1990).
29. E. A. de Andrada e Silva, Phys. Rev. B**46**, 1921 (1992).
30. E. A. de Andrada e Silva, G. C. La Rocca and F. Bassini, Phys. Rev. B**50**, 8523 (1994).
31. B. N. Murdin, C. R. Pidgeon, A. D. Jaroszynski, C. C. Phillips, R. A. Stradling, C. M. Ciesla, R. Praseres and C. J. G. M. Langerak, Submitted to Semiconductor Science and Technology.
32. B. N. Murdin, C. R. Pidgeon, D. A. Jaroszynski, C. C. Phillips, R. A. Stradling, C. M. Ciesla, R. Praseres and G. J. G. M. Langerak Int. Conf. on Narrow Gap Semiconductors (Santa Fe) IoP Conference Series, **144**, 267 (1995).
33. H. K. Choi, S. J. Eglash, App. Phys. Lett.**59**, 1165 (1991).
34. H. K. Choi and S. J. Eglash, App. Phys. Lett. **61**, 1154 (1991).
35. H. Q. Le, G. W. Turner, S. J. Eglash, H. K. Choi and D. A. Coppeta, App. Phys. Lett. **64**, 152 (1994).
36. S. J. Eglash and H. K. Choi, Appl. Phys. Lett. **64**, 833 (1994).
37. S. R. Kurtz, R. M. Bielfeld, L. R. Dawson, K. C. Baucom and A. J. Howard, App. Phys. Lett. **64**, 812 (1994).
38. A. N. Baranov, A. N. Imentkov, V. V. Sherstnev and Y. P. Yakovlev, App. Phys. Lett. **64**, 2480 (1994).
39. R. H. Miles, D. K. Chow, Y. H. Zhang, P. D. Brewer and R. G. Wilson, App. Phys. Lett. **66**, 1921 (1995).
40. Y. H. Zhang, App. Phys. Lett. **66**, 118 (1995) also Int Conf. on Narrow Gap Semiconductors (Santa Fe) IoP Conference Series, **144**, 36 (1995).
41. H. Lee, P. K. York, P. J. Menna, R. U. Martinelli, D. Z. Garbuzov, S. Y. Narayan and J. C. Connolly, App. Phys. Lett. **66**, 1942 (1995).
42. P. J. P. Tang, M. J. Pullin, S. J. Chung, C. C. Phillips, R. A. Stradling, A. G. Norman, Y. B. Li and L. Hart, Semicond. Sci. and Techn. **10**, 1177 (1995).
43. M. J. Pullin, P. J. P. Tang, C. C. Phillips, Y. B. Li, A. G. Norman and R. A. Stradling, Int Conf. on Narrow Gap Semiconductors (Santa Fe) IoP Conference Series, **144**, 8 (1995) also M. J. Pullin, P. J. P. Tang, C. C. Phillips, Y. B. Li, A. G. Norman and R. A. Stradling, SPIE Meeting on Optoelectronics (San Jose) 1995, Vol. 2397, 398.
44. C. Sitori, F. Capasso, J. Faist, D. L. Sivco, A. L. Hutchison and A. Y. Cho, App. Phys. Lett. **66**, 4 (1995).
45. J. Faist, F. Capasso, C. Sitori, D. L. Sivco, A. L. Hutchison and A. Y. Cho, App. Phys. Lett. **66**, 538 (1995).
46. C. Sitori, F. Capasso, J. Faist, D. L. Sivco, A. L. Hutchison and A Y. Cho, App. Phys. Lett. **66**, 3242 (1995).
47. J. M. Arias, M. Zandian, R. Zucca and J. Singh, Semicond. Sci. and Techn. **8**, S255 (1993).
48. H. Q. Le, A. Sanchez, J. M. Arias, M. Zandian, R. R. Zucca and Y. Z. Liu, Int Conf. on Narrow Gap Semiconductors (Santa Fe) IoP Conference Series, **144**, 24 (1995).
49. Z. Shi, M. Tacke, A. Lambrecht and H. Bottner, App. Phys. Lett.**66**, 2537 (1995).
50. E. R. Brown, J. R. Soderstrom, C. D. Parker, L.

J. Mahoney, K. M. Molvar and T. C. McGill, App. Phys. Lett. **58**, 2291 (1991).

51. E. R. Brown, S. J. Eglash, G. W. Turner, C. D. Parker, J. V. Pantano and D. R. Calawa, IEEE Trans on Electron Device **41**, 879 (1994).
52. J. S. Scott, J. P. Kaminski, S. J. Allen, D. H. Chow, M. Lui and T. Y. Lui, Surface Science **305**, 389 (1994).
53. E. Ozbay, D. M. Bloom, D. H. Chow and J. N. Shulman, IEEE Electron Device Letters **14**, 400 (1993).
54. X. Li, K. F. Logenbach, Y. Wang and W. I. Wang, EEE Electron Devices Letters **13**, 192 (1992).
55. C. R. Bolognisi, E. J. Kane and H. Kroemer, IEEE Electron Devices Letters **15**, 16 (1994).
56. J. R. Boos, W. Krupps, D. Park, B. V. Shanabrook and R. Bennett, Electronics Letters **30**, 1983 (1994) and earlier references.
57. J. Heremans, D. L. Partin, C. M. Thrush and L. Green, Semicond. Sci. and Techn. **8**, S424 (1993).